

# Networks with many structural scales: a Renormalization Group perspective

Anna Poggialini,<sup>1,2</sup> Pablo Villegas,<sup>2,3,\*</sup> Miguel A. Muñoz,<sup>4,3</sup> and Andrea Gabrielli<sup>2,5,6</sup>

<sup>1</sup>*Dipartimento di Fisica Università “Sapienza”, P.le A. Moro, 2, I-00185 Rome, Italy.*

<sup>2</sup>*‘Enrico Fermi’ Research Center (CREF), Via Panisperna 89A, 00184 - Rome, Italy*

<sup>3</sup>*Instituto Carlos I de Física Teórica y Computacional, Univ. de Granada, E-18071, Granada, Spain.*

<sup>4</sup>*Departamento de Electromagnetismo y Física de la Materia, Universidad de Granada, Granada 18071, Spain*

<sup>5</sup>*Dipartimento di Ingegneria Civile, Informatica e delle Tecnologie Aeronautiche, Università degli Studi “Roma Tre”, Via Vito Volterra 62, 00146 - Rome, Italy.*

<sup>6</sup>*Istituto dei Sistemi Complessi (ISC) - CNR, Rome, Italy.*

Scale invariance profoundly influences the dynamics and structure of complex systems, spanning from critical phenomena to network architecture. Here, we propose a precise definition of scale-invariant networks by leveraging the concept of a constant entropy loss rate across scales in a renormalization-group coarse-graining setting. This framework enables us to differentiate between scale-free and scale-invariant networks, revealing distinct characteristics within each class. Furthermore, we offer a comprehensive inventory of genuinely scale-invariant networks, both natural and artificially constructed, demonstrating, e.g., that the human connectome exhibits notable features of scale invariance. Our findings open new avenues for exploring the scale-invariant structural properties crucial in biological and socio-technological systems.

The network paradigm effectively captures essential attributes of real-world complex systems, offering a natural framework for approaching entangled interconnected problems across disciplines such as neuroscience [1], ecology [2], and epidemiology [3], among others [4]. Understanding the evolutionary dynamics of complex networks, as they adapt their connectivity pattern to achieve various optimized architectures, is fundamental to understanding their long-term stability or other features determining functional roles and performance [5, 6]. Notably, amidst the multitude of potential network structures, one particular organization ubiquitously arises in natural systems: the scale-free architecture [7–10].

Scale-free networks are characterized by a distribution of node connectivities  $k$  that decays as a power-law  $P(k) \propto k^{-\gamma}$  for large values of  $k$  [7, 11]. In statistical physics, power-law behavior is the hallmark of scale invariance and scaling behavior, implying no significant characteristic value of the analyzed quantity [12–14]. For scale-free networks, there is no typical scale in the degree of connectivity apart from natural cut-offs. To date, the network community has been intrigued by the possibility of discerning, through careful statistical analyses [11, 15], including finite-size effects [16], whether empirical networks genuinely exhibit scale invariance or merely appear to do so. From a theoretical standpoint, addressing this question calls for designing a renormalization group (RG) approach [17–20]. Within such a framework, a fixed point of the RG transformation denotes a state or system whose characteristics remain unchanged under appropriate scale transformations achieved through iterated coarse-graining. RG fixed points are inherently linked to universal scaling laws governing the system, so

systems exhibiting the same fixed point exhibit identical scaling features and are categorized within the same universality class [18, 20]. Hence, a crucial implication of RG theory in statistical physics is the categorization of numerous seemingly disparate physical systems and dynamical models into a relatively compact set of universality classes at criticality, either in or out of thermal equilibrium [21, 22]. Elucidating the relevant ingredients that give rise to a particular universality class offers valuable insights into the fundamental mechanisms underpinning complex systems and their key features.

Given the absence of a natural Euclidean embedding for complex networks, traditional length-scale transformations, exploiting translational invariance, were deemed unfeasible until recently [23, 24]. In particular, small-world effects, evidenced by short path lengths between nodes, further complicate block identification or affine transformations [24–27]. Nevertheless, various techniques have been proposed to tile the network, exploiting specific scale-invariant properties as a function of the number of links along any shortest path between two nodes [23]. These include box-covering methods [27, 28] and embeddings into hyperbolic geometry, which offer a novel approach for understanding complex network structures and dynamics [29, 30]. These approaches often rely on finite-size scaling analysis, which becomes unfeasible for fixed-size networks, complicating their practical application. Consequently, fully characterizing scale-invariant properties in real networks remains an open challenge.

Despite these difficulties, a novel approach known as the Laplacian Renormalization Group (LRG), a generalization of statistical mechanics RG to graphs, has emerged, providing a comprehensive framework for effectively coarse-graining heterogeneous systems in both real space and momentum space [31]. This approach leverages diffusive dynamics on networks to gradually re-

---

\* pablo.villegas@cref.it

move the smallest fine-grained structural scales by progressively eliminating the contribution from large eigenvalues. More specifically, the method allows for the redefinition of effective time-dependent Laplacian and adjacency matrices at progressively coarser scales.

Due to its general validity, it comes natural to propose and study structural scale invariance within the LRG framework, as evidenced by the observation of a time-independent rate of entropy loss [31, 32]. This leads to the still fundamental question of whether non-Euclidean architectures, such as general complex networks, can be intrinsically scale-invariant (see Fig.1). Two key questions arise. Can we identify benchmark classes of network architectures exhibiting genuine scale-invariant behavior defining an analog to universality classes? Can we consequently detect and quantify this kind of self-similarity in real-world networks? Here, we offer a comprehensive definition and an accessible compilation of scale-invariant networks, emphasizing that scale-freeness, i.e., a power law degree distribution, does not imply structural self-similarity. We also analyze actual structural brain networks and highlight their scale-invariant features.

#### Laplacian Renormalization Group (LRG).

The introduction of a multi-scale statistical mechanical approach to heterogeneous networks, the LRG, allows one to detect and describe the different scales that comprise a network [31]. The LRG is based on the time-evolution operator  $e^{-\tau\hat{L}}$  of the diffusion or heat equation, where  $\hat{L} = \hat{D} - \hat{A}$  represents the graph Laplacian operator,  $\hat{A}$  the network adjacency matrix, and  $\hat{D}$  the degree matrix [33]. Using this operator and denoting the Laplacian eigenvalues as  $\lambda_i$  with  $i = 1, \dots, N$  (all of them real and positive [34, 35]), one can define the Laplacian density matrix [36],

$$\hat{\rho}(\tau) = \frac{e^{-\tau\hat{L}}}{Z \equiv \text{Tr}(e^{-\tau\hat{L}})} = \frac{e^{-\tau\hat{L}}}{\sum_{i=1}^N e^{-\lambda_i\tau}}, \quad (1)$$

and develop a "canonical" description of heterogeneous networks in analogy with statistical mechanics [31, 33], where  $\hat{L}$  plays formally the role of a Hermitian Hamiltonian,  $Z(\tau)$  is the partition function, and  $\tau$  is a control scale parameter akin to the inverse temperature.

In this way, as the resolution scale  $\tau$  is increased, the contribution of large eigenvalues to  $\hat{\rho}(\tau)$  -revealing fine structure- is progressively removed, allowing for an effective network coarse-graining [37]. Within this formalism, one can compute the network entropy as  $S(\tau) = -\text{Tr}[\hat{\rho}(\tau) \log \hat{\rho}(\tau)]$ , so that  $S(\tau) = \tau \langle \lambda \rangle_\tau + \ln Z(\tau)$ , where  $\langle \lambda \rangle_\tau \equiv \langle \hat{L} \rangle_\tau = \frac{\sum_{i=1}^N \lambda_i e^{-\tau\lambda_i}}{Z(\tau)}$ . In particular,  $S$  runs from  $S = \ln N$  at  $\tau = 0$ , the segregated (*high temperature*) regime to  $S = 0$  at  $\tau \rightarrow \infty$ , the integrated (*low temperature*) regime. More specifically, one can define the

network entropic susceptibility or "heat capacity" [33]

$$C(\tau) \equiv -\frac{dS}{d \log \tau}, \quad (2)$$

that describes the negative rate of entropy or the rate of information acquired about the network structure during diffusion dynamics at scale  $\tau$ . From the LRG perspective, this can also be seen as the rate at which the complexity of the network shrinks upon coarse-graining. Recalling that in statistical physics, peaks of  $C$  (diverging in the infinite size limit) are associated with structural phase transitions, we can scrutinize  $C$  at varying  $\tau$  to investigate the network multi-scale organization, detecting scales at which entropy changes more significantly due to structural transitions. This description has permitted, for instance, the detection of the information core of a network and its related structural/diffusive transitions [33] and has led to naturally extending the concept of RG to heterogeneous networks [31]. Here, it also allows us to propose informationally *scale-invariant networks* as graphs whose entropy-loss rate  $C(\tau)$  takes a constant value  $C_0 > 0$  across scales or, at least, within a sufficiently broad diffusion-time interval, so that they are approximately scale invariant.

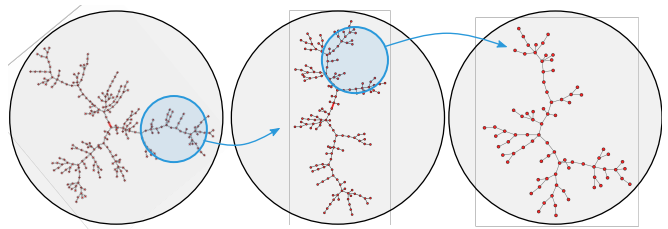


Figure 1. Network splitting in a random tree. The removed link is marked in red, and the zoomed-in region represents the new graph. The intrinsic network properties remain across all scales, showing qualitative evidence of self-similar behavior.

We start demonstrating that this definition of informational scale invariance is satisfied if and only if the Laplacian spectral density can be written as  $w(\lambda) \sim \lambda^\gamma$ , where we have considered the spectral density as a continuum distribution in the infinite size limit. This implies that the macroscopic properties of the network—which stem from vanishing Laplacian eigenvalues—remain invariant under LRG scale transformations. In short, the focus of network scale invariance shifts from a power-law degree distribution to a power-law in the spectral density.

Using Eq.(2) and the definition of  $S(\tau)$  one can derives  $C(\tau) = -\tau^2 \frac{d\langle \lambda \rangle_\tau}{d\tau}$ , and imposing  $C(\tau) = C_0$  to be a constant, one readily gets  $\langle \lambda \rangle_\tau = C_0/\tau$ . It is easy to verify that the only solution to this equation is to assume a Laplacian spectral density  $w(\lambda) \sim \lambda^\gamma$ , so that,

$$C_0 = \frac{\Gamma(\gamma + 2)}{\Gamma(\gamma + 1)} = \gamma + 1 \quad (3)$$

where  $\Gamma(z)$  is the Euler's gamma function. Note that the exponent of the Laplacian spectral density,  $\gamma$ , can be related to the *spectral dimension*,  $d_s$ , which is a global property of the graph, related, e.g., to the infrared singularity of the Gaussian process [38] and that has been shown to provide a robust generalization of the standard dimension for networks [38, 39]. As  $d_s/2 = \gamma + 1$  [38], one concludes that  $C_0$  is constant and equals half of the graph's spectral dimension:  $C_0 = d_s/2$ . Therefore, measuring the heat capacity of a scale-invariant network is an effective method for determining its dimensionality.

Note that, for finite-sized networks, scale invariance is approximate and limited to a finite scale interval. This means that  $C(\tau)$  cannot remain constant across all scales: it decays from its plateau value  $C_0$  to 0 for sufficiently large values of  $\tau$ . To estimate such cut-off, we have to consider that the smallest non-zero eigenvalue  $\lambda_2$  of  $\hat{L}$ , also called "spectral gap" or "Fiedler eigenvalue"  $\lambda_F$ , [40, 41], is the one providing the slowest decaying contribution in time to Eq.(1), therefore determining the asymptotic time decay of  $C(\tau)$ . Starting from Eq.(2) and imposing that the Laplacian spectrum  $\omega(\lambda)$  integrates to  $N$ , we get  $\lambda_F \sim N^{-2/d_s}$  for large  $N$  [42, 43]. From this, it follows (see Supplemental Material, SM [44]),

$$C(\alpha/\lambda_F) \simeq \frac{\Gamma(d_s/2)\Gamma(d_s/2 + 2, \alpha) - \Gamma^2(d_s/2 + 1, \alpha)}{\Gamma^2(d_s/2)}, \quad (4)$$

where  $\Gamma(x, \alpha) = \int_\alpha^\infty du u^{x-1} e^{-u}$  is the lower incomplete Euler Gamma function which exponentially decreases in  $\alpha$  for  $\alpha \gg 1$ . This permits a complementary way to estimate  $d_s$  from finite-size scaling of  $C(\tau)$  in finite-scale-invariant networks. For practical purposes, this can be done by studying the scaling in  $N$  of  $\tau$  in the large time-decaying region for which  $C$  gets a fixed value. Here, we use the value  $C = 1/2$ , denoted as  $\tau_F$ .

#### Laplacian Random-Walk renormalization group

The LRG method relies on a "heat-like" diffusion process defined by  $\hat{L}$ . However, we wonder whether the results obtained for scale invariance and graph dimensionality hold if we use the Laplacian random-walk operator,  $\hat{L}_{RW} = \hat{D}^{-1}\hat{L}$  instead of  $\hat{L}$ .  $\hat{L}_{RW}$  describes the time-discrete dynamics of a RW moving from a node to any nearest neighbor node with uniform probability, i.e.,  $\hat{L}_{RW}$  represents the transition matrix for the RW dynamics on a graph [34, 45]. We emphasize that, even if  $\hat{L}_{RW}$  is not symmetric, it is equivalent to the symmetric operator  $\hat{L}_{sym} = D^{1/2}\hat{L}_{RW}\hat{D}^{-1/2}$  [34] with all its eigenvalues real and satisfying  $0 \leq \mu_i \leq 2$ . We can, thus, reformulate the LRG for the RW dynamics by substituting  $\hat{L}$  with  $\hat{L}_{sym}$ . For clarity, we define the related heat capacities as  $C_L$  and  $C_R$ , respectively. The operator  $\hat{L}_{RW}$  provided the original definition of the random-walk spectral dimension,  $d_s^{RW}$ , related to the first-return time distribution of the random walker  $P_0(t)$  [38, 46] by the scaling  $P_0(t) \propto t^{-d_s^{RW}/2}$ . This is the original extension of the

behavior on  $d$ -dimensional lattices where  $P_0(t) \propto t^{-d/2}$  [47]. Even if  $\hat{L}$  or  $\hat{L}_{RW}$  are known to coincide in regular networks such as lattices, both operators can unravel heterogeneous network structures in different ways [48] and, to our knowledge, there is no proof that  $d_s = d_s^{RW}$  for generic heterogeneous networks.

**LRG non-trivial fixed points.** In what follows, we tackle the following lingering questions: What are the current non-trivial fixed points of LRG, i.e., families or "universality classes" of scale-invariant networks? Are scale-invariant networks necessarily scale-free?

To start, let us remark that, as shown in SM [44], regular or homogeneous lattices, with a degree distribution  $P(\kappa) = \delta(\kappa - \kappa_0)$ , represent the simplest case of scale-invariant structures lacking scale-free properties. However, our main focus is categorizing *heterogeneous* and *stochastic* scale-invariant networks.

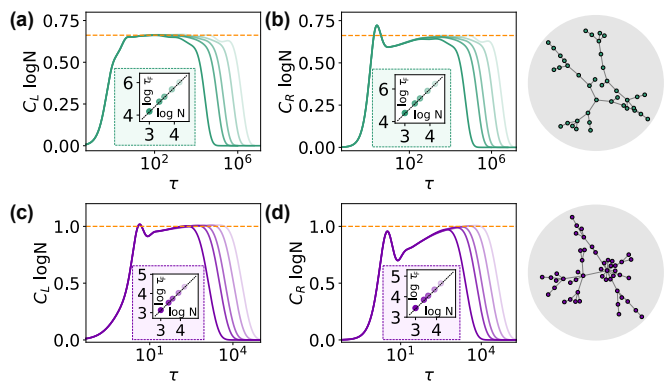


Figure 2. **Trees.** heat capacity versus diffusion time for: (a)-(b) RTs and (c)-(d) BA networks with  $m = 1$ . We have used  $\hat{L}$  in (a) and (c) and  $\hat{L}_{RW}$  in (b) RTs and (d). Insets show the scaling of  $\tau_F$  as a function of the network size  $N$ . Orange dashed lines and solid black lines represent the theoretical expectation, using  $d_s^{RT} = 4/3$  and  $d_s^{BA} = 2$ . All curves have been averaged over  $10^3$  independent realizations. Different colors represent different sizes  $N = \{1, 2.5, 4, 8, 16\} \times 10^3$ .

The **first** category of self-similar networks comprises trees, i.e., connected loopless networks. It is known that the spectral dimension of random trees, with minimal branching ratio  $b_{min} = 1$ , depends upon the first two moments of the degree distribution  $P(\kappa)$  [49, 50]. Specifically,  $d_s = 4/3$  if  $\langle \kappa^2 \rangle$  is finite, while the problem remains open when  $\langle \kappa^2 \rangle$  diverges [49, 51, 52]. Here, we examine two specific cases within the lenses of LRG: ordinary random trees (RT) and Barabási-Albert (BA) networks where new nodes attach preferentially to existing nodes, forming  $m = 1$  edges [7]. As reported in Fig.2(a),  $C_L$  shows a plateau corresponding to the theoretically known spectral dimension for RTs,  $d_s = 4/3$  [51] and obeying the finite-size scaling condition, Eq.(4). Also, we observe that  $\hat{L}_{RW}$  does not alter this value (see Fig.2(b)), despite specific differences in the susceptibility shape, as the local

peak at short times in Fig.2(b).

Instead, BA networks (with  $m = 1$ ) have a constant heat capacity corresponding to a spectral dimension  $d_s = 2$  (see Fig.2(c) and the inset) as in this case  $\langle \kappa^2 \rangle$  diverges. As shown in Fig.2(d),  $C_R$  grows linearly in the intermediate regime, finally becoming flat for asymptotic times as the network size is increased, confirming the intrinsic scale-invariant structure, with  $d_s^{RW} = d_s = 2$ . We stress that the same spectral dimension is also obtained for Bethe lattices with coordination number  $z \geq 3$  (see [53] and SM [44]) for a different reason: in this case  $b_{min} = k_0 - 1 \geq 2$ . Besides, BA networks with any value of  $m > 1$  show no sign of scale invariance (see SM [44]), proving that the archetypes of scale-free networks are not scale invariant. This prevents preferential attachment from generating self-similar networks with  $d_s > 2$ .

**Second**, we consider networks that, contrary to trees, exhibit a non-vanishing clustering coefficient. In particular, we analyze Dorogovstev-Golstev-Mendes [54] networks and their generalization:  $(u,v)$ -flowers [24, 54, 55]. These deterministic fractal-like structures grow by iteratively replacing the link between two nodes with two paths of lengths  $u$  and  $v$ , respectively (see SM [44]). Diameter-based analyses such as calculating the Hausdorff dimension of these networks seem to lead to an apparent paradox: all  $(1, v)$  flowers are infinite-dimensional and exhibit anomalous scaling functions [24, 54, 56]. This paradox stems from the lack of network embedding in an Euclidean space. Conversely, as shown in Figs.3(a), (b) and SM [44], all flowers exhibit well-defined spectral dimensions [24],  $d_s = \log(u + v) / \log(uv)$  ranging from  $d_s \approx 3.17$  to  $d_s = 1$ . Fig.3(b) sheds much light on their differences:  $(u,v)$ -flowers with  $u > 1$  exhibit characteristic oscillations emerging from the discrete nature of the recursive network growth process (much as log-periodic oscillations in standard fractal analyses of deterministic structures, as stem from their discrete scale invariance [13, 57]). Thus, we demonstrate that  $C$  can detect the presence of discrete scale invariance on networks.

**Third**, to investigate whether the self-similarity of network models can be present in stochastic scale-free graphs even if they exhibit small-world properties [24], we consider the Kim and Holme (KH) model [58]. This consists of modifying BA networks with a probability  $p$  that each newly added node forms a triangle with existing ones (see SM [44]). These networks show both a power-law degree distribution and a high clustering coefficient. Our analysis of KH networks evidences that they are scale-invariant only for the particular choice  $p = 1$ . Indeed, as shown in Figs.3(c) and (d),  $C_R$  (and  $C_L$  [44]) shows a plateau with spectral dimension ranging from  $d_s = 2.57(1)$  to  $d_s = 3.65(1)$  as  $m$  is increases (see SM [44]).

**Fourth**, we have investigated the behavior of networks where a hierarchical structure is built in by construction. In particular, we have analyzed the so-called Dyson graph [59, 60]: a fully connected deterministic graph where

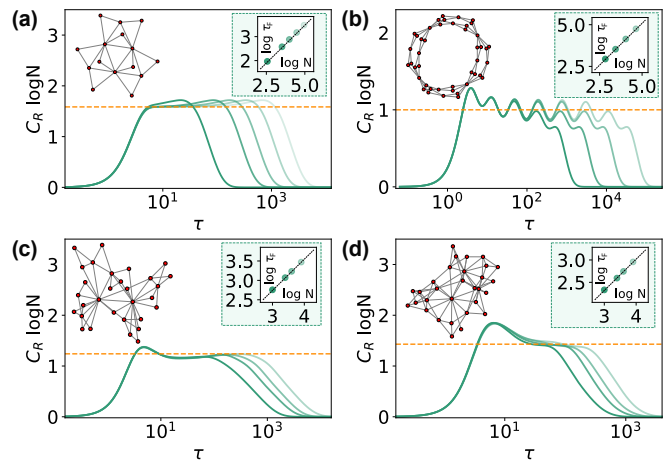


Figure 3. **Clustered networks.** RW heat capacity versus diffusion time for: (a) (1,2) flowers of sizes  $s=6,8,9,10,11$ , (b) (2,2) flowers of sizes  $s=5,6,7,8$ . For  $(u,v)$  flowers, the number of nodes is  $N_s = \left( \frac{w}{w-1} + \frac{w-2}{w-1} w^s \right)$ , with  $w = u + v$ . (c) KH with  $m = 2$  and (d) KH with  $m = 3$  of sizes  $N = \{1, 2.5, 4, 8\} \times 10^3$ . Insets show the scaling  $\tau_F$  as a function of the system size. Orange dashed lines and solid black lines represent the theoretical expectation. All curves have been averaged over  $10^3$  independent realizations.

weights of links are hierarchically organized (see SM [44]). It has a spectral dimension  $d_s = 2 / (2\sigma - 1)$  where  $\sigma$  is a scaling parameter controlling the weight strength at every scale. Fig.4(a) shows the constant plateau of  $C_L$  for a Dyson network with  $\sigma = 0.85$ , in agreement with the theoretical value. We have also considered hierarchical modular networks (HMNs) that were proposed using inspiration from actual brain networks [61]. In HMNs, nodes grouped in basal fully-connected modules are recursively coupled with nodes in other moduli, establishing inter-modular links randomly, in a hierarchical fractal-like way (see SM [44]). Fig.4(b) shows their heat capacity: HMNs are always scale-invariant for any set of parameters, with spectral dimension ranging in the interval  $d_s \in (1.25, 2)$  (see SM [44]).

**Finally**, we have analyzed the Human Connectome (HC) structural network [1]. To address the issue that these empirical networks are usually single realizations of a fixed size, we have applied the LRG framework [31] to analyze reduced versions of the HC network, performing finite-size scaling analysis. As the weighted HC network is a dense structure presenting many weak links, one needs to sparsify the network by removing links below a certain threshold, searching for scale-invariant features while avoiding generating a trivial random tree (as expected to emerge at the percolation critical point for every weighted network; see SM [44]). The analysis of  $C_L$  for the thresholded HC network is displayed in Fig.4(c), while Fig.4(d) shows the finite-size scaling of  $\lambda_F$  for reduced versions of the HC. Both analyses support an un-

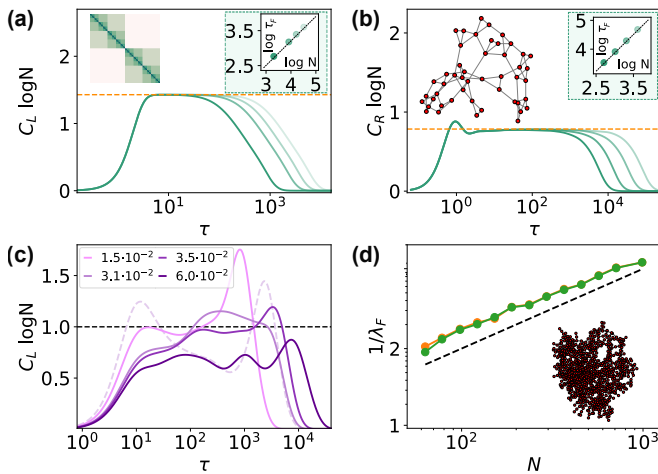


Figure 4. **Hierarchical networks.** Heat capacity versus diffusion time for: (a) Dyson graphs of sizes  $s = 11, 13, 14, 15$  and  $\sigma = 0.85$ . The upper left inset shows the weighted adjacency matrix. (b) HMNs with  $m_0 = 3$  and  $\alpha = 2$ , for sizes  $s = 9, 10, 11, 12$ . System sizes correspond to  $N = 2^s$  in both cases. Insets show the scaling of  $\tau_F$  as a function of  $N$ . Orange dashed and solid black lines represent the theoretical expectation. (c) The HC for different thresholds (see legend). (d) The scaling of  $\tau_F$  for coarse-grained versions of the HC with  $T = 3 \cdot 10^{-2}$  and different fixed values of  $\tau = 10^{-1}, 10^0$ , and  $10^1$ . The black dashed line corresponds to  $d_s = 1.9$ .

derlying topology with spectral dimension  $d_s \sim 1.9(1)$ .

**Outlook.** The observation of scale-invariance along length and time scales gave rise to one of the most potent tools in theoretical physics in the last 50 years: the RG [18, 20]. In Kadanoff's words [62]: "*All phase transition problems can be divided into a small number of different classes depending upon the dimensionality of the system and the symmetries of the order state*". Indeed, the initial implementation of RG ideas took advantage of the geometrical homogeneity and translational invariance of Euclidean lattices to perform scaling of statistical physical systems, computing related critical exponents [63], and leading to a categorization of apparently diverse phase transitions into a few universality classes [21, 22].

Extending the concept of universality to networks with heterogeneous and non-local connectivity properties has long challenged network scientists. Even though remarkable advances have been recently made [27–30, 64, 65], a full understanding of scale-invariance in generic networks remains an open problem. Initially, network scale-invariance was assimilated with power-law degree distributions [16]. However, as we explicitly show, *scale-freeness* of node degrees is neither necessary nor sufficient for networks to exhibit true self-similarity [11].

Using the recently formulated LRG [31, 33], we propose a general framework to characterize and classify the *non-trivial* structural fixed points, in the jargon of the RG, by describing their scaling properties. In short, a constant heat capacity value suggests the presence of scale-

invariant or macroscopically self-similar graphs, reflecting a constant entropy-loss rate for all network scales. First, in the light of the LRG, we have connected the constant entropy-loss rate with the original concept of spectral dimension, confirming its goodness as a natural generalization of Euclidean dimension [38, 39, 46]. We have also shed light on a crucial open problem by showing the uniqueness of  $d_s$  when using either  $\hat{L}$  or  $\hat{L}_{RW}$ . Therefore, we can hypothesize that the spectral dimension is a universal inherent property of any graph that constitutes a first characterization of it. Analogously, as with what happens in fractals, specifying the spectral dimension does not uniquely determine dynamic properties on top of the network. To characterize them, further aspects or exponents (like fractal lacunarity or porosity). Our LRG analysis allows us to identify regular lattices, trees, clustered networks, and hierarchical networks as basic classes or categories of scale-invariant networks. Beyond the trivial case of regular lattices, we emphasize the relevance of (u-v)-flowers and KH networks as singular structures combining local clustering and hubs at all scales to generate self-similar topologies. Instead, trees are bound to have  $d_s \leq 2$ , and the only inclusion of hubs seems insufficient to achieve high-dimension values. As a general statement, the higher the dimension, the higher the difficulty in generating self-similar heterogeneous networks [24]. However, our results bear promising for scrutinizing biological and socio-technological networks. Hierarchical networks, naturally proposed in the brain community as an optimal architecture for information processing, exhibit scale-invariant properties [65]; we evidence well-defined scaling properties for the HC [66, 67], with  $d_s \approx 1.9(1)$ , validating recent theoretical proposals, such as HMNs, to describe their structure [61]. Finally, we are confident that our results will be a solid ground for future dynamical RG theoretical calculations on these structures and for detecting signs of scale-invariance in real networks or synthetic models.

## ACKNOWLEDGMENTS

The authors thank T.Gili, D. Cassi, and R. Burioni for very useful discussions and comments. P.V. and M.A.M. acknowledge financial support from the Spanish "Ministerio de Ciencia, Innovación y Universidades" and the "Agencia Estatal de Investigación (AEI)" under Project Ref. PID2020-113681GB-I00 funded by MICIN/AEI/10.13039/501100011033.

- [1] A. Fornito, A. Zalesky, and E. Bullmore, *Fundamentals of brain network analysis* (Academic press, 2016).
- [2] J. Bascompte, *Basic Appl. Ecol.* **8**, 485 (2007).
- [3] R. Pastor-Satorras and A. Vespignani, *Phys. Rev. Lett.* **86**, 3200 (2001).
- [4] M. E. Newman, *SIAM Rev.* **45**, 167 (2003).

- [5] M. A. Fortuna, J. A. Bonachela, and S. A. Levin, *Proc. Natl. Acad. Sci. U.S.A.* **108**, 19985 (2011).
- [6] P. Villegas, M. A. Muñoz, and J. A. Bonachela, *J. R. Soc. Interface.* **17**, 20190845 (2020).
- [7] A.-L. Barabási and R. Albert, *Science* **286**, 509 (1999).
- [8] M. Newman, *Networks: An Introduction* (Oxford University Press, Oxford, 2010).
- [9] A. Barabási, *Network Science* (Cambridge University Press, Cambridge, 2016).
- [10] G. Caldarelli, A. Capocci, P. De Los Rios, and M. A. Muñoz, *Phys. Rev. Lett.* **89**, 258702 (2002).
- [11] A. D. Broido and A. Clauset, *Nat. Comm.* **10**, 1017 (2019).
- [12] M. E. Newman, *Contemp. Phys.* **46**, 323 (2005).
- [13] D. Sornette, *Critical phenomena in natural sciences: chaos, fractals, selforganization and disorder: concepts and tools* (Springer-Verlag Berlin Heidelberg, 2006).
- [14] M. A. Muñoz, *Rev. Mod. Phys.* **90**, 031001 (2018).
- [15] A. Clauset, C. R. Shalizi, and M. E. Newman, *SIAM Rev.* **51**, 661 (2009).
- [16] M. Serafino, G. Cimini, A. Maritan, A. Rinaldo, S. Suweis, J. R. Banavar, and G. Caldarelli, *Proc. Natl. Acad. Sci. U.S.A.* **118**, e2013825118 (2021).
- [17] K. G. Wilson, *Sci. Am.* **241**, 158 (1979).
- [18] D. J. Amit and V. Martin-Mayor, *Field Theory, the Renormalization Group, and Critical Phenomena*, 3rd ed. (World Scientific, Singapore, 2005).
- [19] G. Caldarelli, T. Gili, A. Gabrielli, and P. Villegas, *arXiv preprint arXiv:2406.02337* (2024).
- [20] M. Kardar, *Statistical physics of fields* (Cambridge University Press, Cambridge, 2007).
- [21] P. C. Hohenberg and B. I. Halperin, *Rev. Mod. Phys.* **49**, 435 (1977).
- [22] G. Ódor, *Rev. Mod. Phys.* **76**, 663 (2004).
- [23] F. Radicchi, J. J. Ramasco, A. Barrat, and S. Fortunato, *Phys. Rev. Lett.* **101**, 148701 (2008).
- [24] H. D. Rozenfeld, S. Havlin, and D. Ben-Avraham, *New J. Phys.* **9**, 175 (2007).
- [25] R. Cohen and S. Havlin, *Phys. Rev. Lett.* **90**, 058701 (2003).
- [26] D. J. Watts and S. H. Strogatz, *Nature* **393**, 440 (1998).
- [27] H. D. Rozenfeld, C. Song, and H. A. Makse, *Phys. Rev. Lett.* **104**, 025701 (2010).
- [28] C. Song, S. Havlin, and H. A. Makse, *Nature* **433**, 392 (2005).
- [29] M. A. Serrano, D. Krioukov, and M. Boguñá, *Phys. Rev. Lett.* **100**, 078701 (2008).
- [30] G. García-Pérez, M. Boguñá, and M. Á. Serrano, *Nat. Phys.* **14**, 583 (2018).
- [31] P. Villegas, T. Gili, G. Caldarelli, and A. Gabrielli, *Nat. Phys.* **19**, 445–450 (2023).
- [32] K. Klemm, *Nat. Phys.* **19**, 318 (2023).
- [33] P. Villegas, A. Gabrielli, F. Santucci, G. Caldarelli, and T. Gili, *Phys. Rev. Research* **4**, 033196 (2022).
- [34] F. R. Chung, *Spectral graph theory*, Vol. 92 (American Mathematical Soc., Providence, 1997).
- [35] L. Donetti, F. Neri, and M. A. Muñoz, *J. Stat. Mech.: Theory Exp.* **2006** (08), P08007.
- [36] M. De Domenico and J. Biamonte, *Phys. Rev. X* **6**, 041062 (2016).
- [37] This idea is also at the basis of different community detection algorithms [48, 68–70].
- [38] R. Burioni and D. Cassi, *Phys. Rev. Lett.* **76**, 1091 (1996).
- [39] D. Cassi, *Phys. Rev. Lett.* **68**, 3631 (1992).
- [40] M. Fiedler, *Banach Center Publications* **1**, 57 (1989).
- [41] F. Chung, L. Lu, and V. Vu, *Proc. Natl. Acad. Sci. USA* **100**, 6313 (2003).
- [42] K. C. Das, *Comput. Math. Appl.* **48**, 715 (2004).
- [43] S. N. Dorogovtsev and J. F. Mendes, *The nature of complex networks* (Oxford University Press, 2022).
- [44] See Supplemental Material at [].
- [45] R. Burioni and D. Cassi, *J. Phys. A* **38**, R45 (2005).
- [46] D. Cassi and L. Fabbian, *J. Phys. A* **32**, L93 (1999).
- [47] S. Alexander and R. Orbach, *J. Phys. Lett.* **43**, 625 (1982).
- [48] P. Villegas, A. Gabrielli, A. Poggialini, and T. Gili, *arXiv* (2023), 2301.04514.
- [49] L. Donetti and C. Destri, *J. Phys. A Math. Gen.* **37**, 6003 (2004).
- [50] Z. Burda, J. D. Correia, and A. Krzywicki, *Phys. Rev. E* **64**, 046118 (2001).
- [51] C. Destri and L. Donetti, *J. Phys. A Math. Gen.* **35**, 9499 (2002).
- [52] S. N. Dorogovtsev, A. V. Goltsev, J. F. Mendes, and A. N. Samukhin, *Phys. Rev. E* **68**, 046109 (2003).
- [53] A. Erzan and A. Tuncer, *Linear Algebra Its Appl.* **586**, 111–129 (2020).
- [54] S. N. Dorogovtsev, A. V. Goltsev, and J. F. F. Mendes, *Phys. Rev. E* **65**, 066122 (2002).
- [55] H. D. Rozenfeld, L. K. Gallos, C. Song, and H. A. Makse, Fractal and transfractal scale-free networks, in *Encyclopedia of Complexity and Systems Science*, edited by R. A. Meyers (Springer, New York, 2009) pp. 3924–3943.
- [56] J. Peng and E. Agliari, *Chaos* **27**, 083108 (2017).
- [57] T. Vicsek, M. Shlesinger, and M. Matsushita, *Fractals in Natural Sciences* (World Scientific, Singapore, 1994).
- [58] P. Holme and B. J. Kim, *Phys. Rev. E* **65**, 026107 (2002).
- [59] F. J. Dyson, *Commun. Math. Phys.* **12**, 91 (1969).
- [60] E. Agliari and F. Tavani, *Sci. Rep.* **7**, 39962 (2017).
- [61] P. Moretti and M. A. Muñoz, *Nat. Comm.* **4**, 2521 (2013).
- [62] L. P. Kadanoff, in *Proceedings of the Enrico Fermi Summer School of Physics, Varenna 1970*, edited by M. S. Green (Academic Press, London and New York, 1971).
- [63] K. G. Wilson and M. E. Fisher, *Phys. Rev. Lett.* **28**, 240 (1972).
- [64] C. Song, S. Havlin, and H. A. Makse, *Nature* **433**, 392 (2005).
- [65] M. Zheng, A. Allard, P. Hagmann, and M. Á. Serrano, *Proc. Natl. Acad. Sci. USA* **117**, 20244 (2020).
- [66] O. Sporns, D. R. Chialvo, M. Kaiser, and C. C. Hilgetag, *Trends Cogn. Sci.* **8**, 418 (2004).
- [67] P. Hagmann, L. Cammoun, X. Gigandet, R. Meuli, C. J. Honey, V. J. Wedeen, and O. Sporns, *PLoS Biol.* **6**, e159 (2008).
- [68] A. Arenas, A. Díaz-Guilera, and C. J. Pérez-Vicente, *Phys. Rev. Lett.* **96**, 114102 (2006).
- [69] L. Donetti and M. A. Muñoz, *J. Stat. Mech.: Theory Exp.* **2004** (10), P10012.
- [70] L. Donetti, P. I. Hurtado, and M. A. Muñoz, *Phys. Rev. Lett.* **95**, 188701 (2005).

# Supplemental Material: Networks with many structural scales: a Renormalization Group perspective

Anna Poggialini,<sup>1,2</sup> Pablo Villegas,<sup>2,3,\*</sup> Miguel A. Muñoz,<sup>4,3</sup> and Andrea Gabrielli<sup>2,5</sup>

<sup>1</sup>*Dipartimento di Fisica Università “Sapienza”, P.le A. Moro, 5, I-00185 Rome, Italy.*

<sup>2</sup>*‘Enrico Fermi’ Research Center (CREF), Via Panisperna 89A, 00184 - Rome, Italy*

<sup>3</sup>*Instituto Carlos I de Física Teórica y Computacional,  
Universidad de Granada, E-18071, Granada, Spain.*

<sup>4</sup>*Departamento de Electromagnetismo y Física de la Materia, Universidad de Granada, Granada 18071, Spain*

<sup>5</sup>*Dipartimento di Ingegneria Civile, Informatica e delle Tecnologie Aeronautiche,  
Università degli Studi “Roma Tre”, Via Vito Volterra 62, 00146 - Rome, Italy.*

## CONTENTS

1. Asymptotic limit of $\lambda_F$	2
2. Asymptotically scale-invariant graphs	3
3. Regular lattices	3
4. Scale-dependent networks	4
5. Bethe lattices	5
6. Barabási-Albert networks	6
7. $(u, v)$ –flowers	7
8. Kim and Holme networks	9
9. Dyson network	10
10. HMN networks	11
11. Human Connectome network	13
References	14

---

\* pablo.villegas@cref.it

## 1. ASYMPTOTIC LIMIT OF $\lambda_F$

Let us assume to have a scale-invariant network for which  $\omega(\lambda) = A\lambda^\gamma$ , with  $\gamma = d_s/2 - 1$  and that  $\lambda_{max}$  do not depend on  $N$  (reasonable if the maximum node degree does not scale with  $N$ ) [1]. Since the total number of eigenvalues is  $N$ , i.e. the number of network nodes, we have

$$A \int_0^{\lambda_{max}} d\lambda \lambda^\gamma \equiv A \frac{\lambda_{max}^{\gamma+1}}{\gamma+1} = N,$$

which implies  $A = \frac{\gamma+1}{\lambda_{max}} N$ . On the other hand, by the definition of the Fiedler eigenvalue  $\lambda_F$ , we need to have [2],

$$A \int_0^{\lambda_F} d\lambda \lambda^\gamma = 1,$$

from which we can derive the scaling relation  $\lambda_F \sim N^{-2/d_s}$ .

Under these hypotheses, the specific heat can be written as

$$C(t) = t^2 \left( \langle \lambda^2 \rangle_t - \langle \lambda \rangle_t^2 \right) = t^2 \frac{\left( A \int_0^{\lambda_{max}} d\lambda \lambda^\gamma e^{-\lambda t} \right) \left( A \int_{\lambda_F}^{\lambda_{max}} d\lambda \lambda^{\gamma+2} e^{-\lambda t} \right) - \left( A \int_{\lambda_F}^{\lambda_{max}} d\lambda \lambda^{\gamma+1} e^{-\lambda t} \right)^2}{\left( A \int_0^{\lambda_{max}} d\lambda \lambda^\gamma e^{-\lambda t} \right)^2}, \quad (1)$$

where the lower integration extreme for the integrals of the first and second moments of  $\lambda$  with time dependent measure  $\hat{\rho}(t)$  is explicitly limited to  $\lambda_F$  as the fundamental eigenvalue  $\lambda = 0$  does not contribute and in this way we can explicitly study the effect of the  $N$ -dependent gap  $\lambda_F \sim N^{-2/d_s}$  for finite  $N$ .

By the change of integration variable  $u = \lambda t$ , we can write

$$C(t) = \frac{\left( \int_0^{u_{max}} du u^\gamma e^{-u} \right) \left( \int_{\lambda_F t}^{u_{max}} du u^{\gamma+2} e^{-u} \right) - \left( \int_{\lambda_F t}^{u_{max}} du u^{\gamma+1} e^{-u} \right)^2}{\left( \int_0^{u_{max}} du u^\gamma e^{-u} \right)^2} \quad (2)$$

with  $u_{max} = \lambda_{max} t$ .

Let us now evaluate  $C(t_F)$  with  $t_F = \alpha/\lambda_F \sim N^{2/d_s}$  where  $C(t)$  is expected to deviate from the constant value  $d_s/2$  because of finite size effects giving a constant gap. In this case, due to the exponential factor in the integrals, we can take with no danger  $u_{max} \rightarrow +\infty$ . Consequently, we can write

$$C(\alpha/\lambda_F) = \frac{\Gamma(\gamma+1) \int_\alpha^\infty du u^{\gamma+2} e^{-u} - \left( \int_\alpha^\infty du u^{\gamma+1} e^{-u} \right)^2}{\Gamma^2(\gamma+1)} = \frac{\Gamma(\gamma+1)\Gamma(\gamma+3, \alpha) - \Gamma^2(\gamma+2, \alpha)}{\Gamma^2(\gamma+1)}, \quad (3)$$

where  $\Gamma(x)$  is the complete Euler Gamma function and  $\Gamma(x, \alpha) = \int_\alpha^\infty du u^{x-1} e^{-u}$  is the lower incomplete Euler Gamma function. Equation (3) immediately shows that for different  $N$  we get the same large time value for the specific heat  $C(t)$ , different from the infinite  $N$  value  $d_s/2$ , at corresponding times  $t = \alpha/\lambda_F$  where  $\lambda_F \sim N^{-2/d_s}$ , while this value depends on  $\alpha$ . In particular, by using the large  $\alpha$  asymptotic expansion of  $\Gamma(x, \alpha)$  in Eq. (3) we get that the main  $\alpha$  dependence characterized by the following exponential decay:

$$C(\alpha/\lambda_F) = \frac{\alpha^{\gamma+2} e^{-\alpha}}{\Gamma(\gamma+1)}. \quad (4)$$

Finally, it is simple to note that in the limit  $\alpha \rightarrow 0^+$  Eq. (3) correctly coincides with the limit  $N \rightarrow \infty$  of Eq. (2) at finite  $t$ :

$$C(t) = \frac{\Gamma(\gamma+1)\Gamma(\gamma+3) - [\Gamma(\gamma+2)]^2}{[\Gamma(\gamma+1)]^2} = \gamma+1 = d_s/2,$$

which explains the plateau value.

## 2. ASYMPTOTICALLY SCALE-INVARIANT GRAPHS

Despite its simplicity, the request for a unique power-law behavior to hold on to all the support of the spectrum may seem too severe to be easily detected in both synthetic and real graphs. However, a large set of networks satisfies a much weaker but equally relevant condition:  $\omega(\lambda) \sim \lambda^\gamma$  in the limit  $\lambda \rightarrow 0$ . Networks that meet this asymptotic condition are scale-invariant graphs. The results shown in the main text can be derived, in a more general way, for the asymptotic case using the Tauberian and Abelian theorems [3]. In particular, one can write

$$C(t)\log(N) = -t^2 \frac{d}{dt} h(t). \quad (5)$$

If  $\omega(\lambda) \sim \lambda^\gamma$  in for  $\lambda \rightarrow 0$ , then  $h(t) \sim t^{-1}$  in the limit  $t \rightarrow \infty$  and  $C(t)\log(N) \sim \gamma + 1 < \infty$  in the same regime. In this context, the study of the spectral dimension  $d_s$  fits the well-known asymptotic definitions  $d_s = -2 \lim_{t \rightarrow \infty} \frac{\ln p_t(G,v)}{\ln t}$  and  $\lim_{\lambda_N \rightarrow 0} \omega_N(\lambda_N)$  when these limits exist for infinite-sized graphs and where  $p_t(G,v)$  is the return probability of a random walk to a generic vertex  $v$  at time  $t$  and  $\omega_N(\lambda_N)$  is the spectral density of normalized Laplacian operator.

## 3. REGULAR LATTICES

For consistency and to avoid spurious results, we first study the most straightforward trivial scale-invariant structures: regular lattices. As shown in Figure 1, the  $\tau$  peak at short diffusion times reflects the characteristic resolution scale of the system (or, in other words, the 'cutoff' scale,  $\Lambda$ ). We have analyzed different simple cases (both in 2D and 3D) to check the correspondence between the specific heat and the expected dimension of the network, using both  $\hat{L}$  and  $\hat{L}_{RW}$ . We emphasize that, in this particular case, both Laplacians are formally equivalent, as for regular lattices,  $P(\kappa) = \delta(\kappa - \kappa_0)$ , where  $k_0$  represents the coordination number of the homogeneous structure.

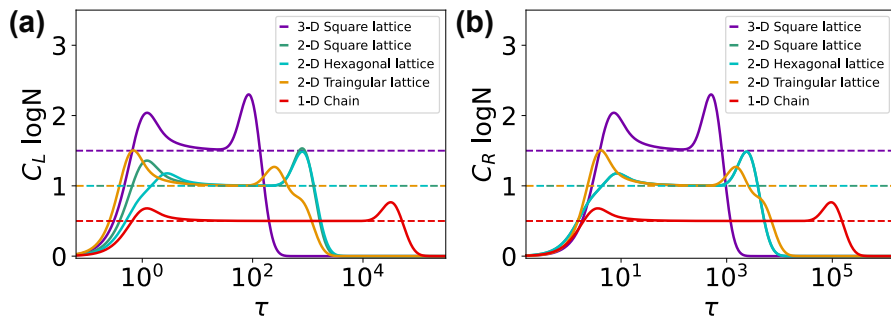


FIG. 1. **Regular lattices.** Specific heat versus diffusion time by using (a)  $\hat{L}$  and (b)  $\hat{L}_{RW}$ . All networks show a plateau for the expected dimension of any lattice for both cases.

## 4. SCALE-DEPENDENT NETWORKS

We have conducted extensive simulations to analyze the specific heat of Erdős-Rényi networks of different mean connectivity. Figure 2 shows the expected specific heat versus the diffusion time for different sizes of the system, which shows that there is no scaling for large networks. Note also that  $C_L$  presents a single peak, pointing to a scale that corresponds to the system size.

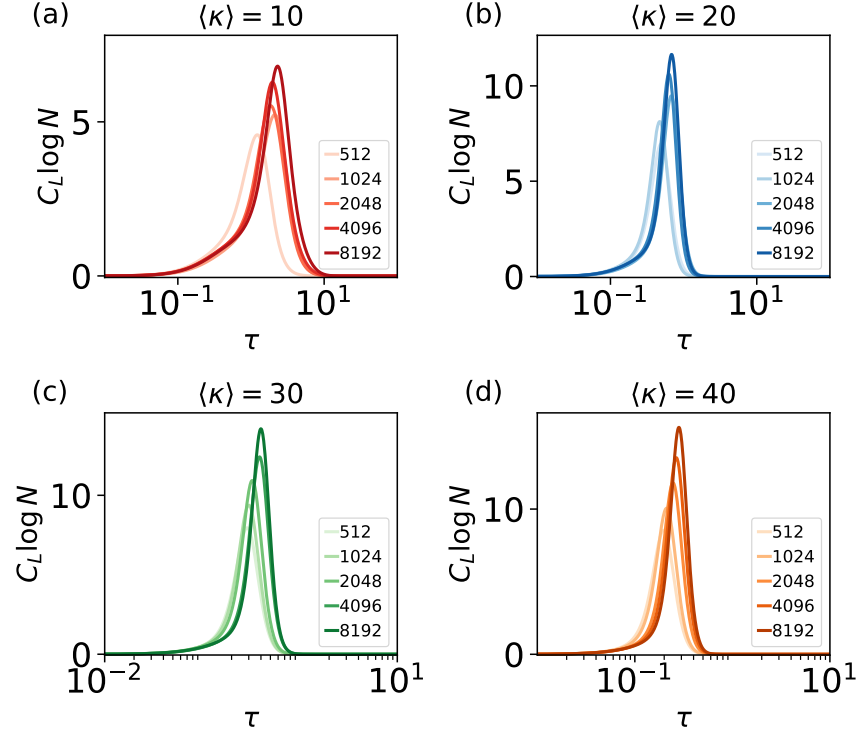


FIG. 2. **Erdős-Rényi networks.** Specific heat versus diffusion time for different network sizes (see legend) and mean connectivity: (a)  $\langle \kappa \rangle = 10$ , (b)  $\langle \kappa \rangle = 20$ , (c)  $\langle \kappa \rangle = 30$ , (d)  $\langle \kappa \rangle = 40$ . All curves have been averaged over  $10^2$  network realizations.

## 5. BETHE LATTICES

One of the paradigmatic cases of self-similar networks is those of Bethe lattices with coordination number  $z > 2$ . Figure 3 shows the specific heat for different Bethe lattices with coordination numbers  $z = 3, 4, 5$  and 6. Note that the specific heat monotonically grows for all networks at short times. Still, the heat capacity asymptotically converges to a constant value with a spectral dimension  $d_S = 2$  (see Figure 3). The scaling of the Fiedler eigenvalue confirms such a constant value (see also the theoretical proof below), as reported in Figure 4.

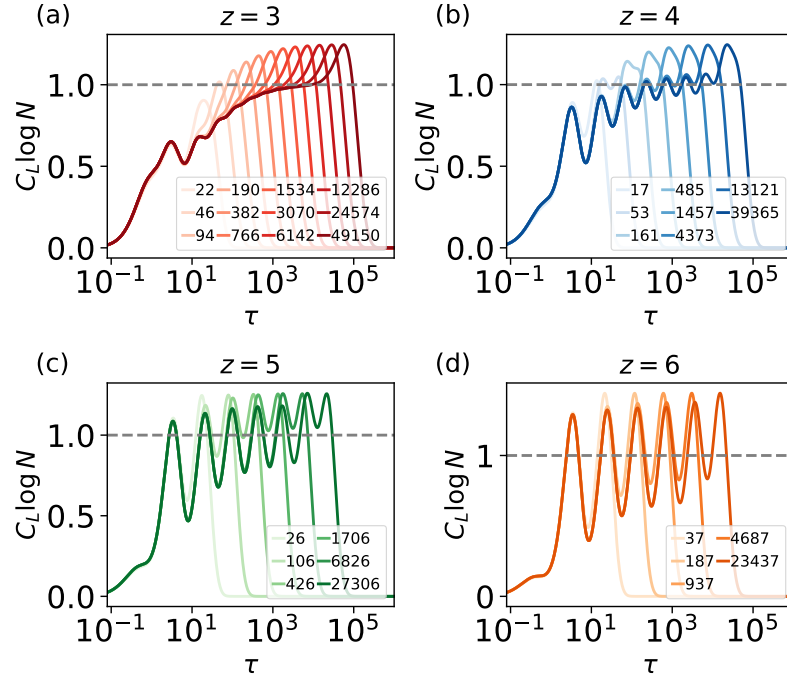


FIG. 3. **Bethe lattice.** Specific heat versus system size for Bethe lattices of different coordination numbers: (a)  $z = 3$ , (b)  $z = 4$ , (c)  $z = 5$ , (d)  $z = 6$ . The dashed gray line shows the value associated with the scaling of the Fiedler eigenvalue in Figure 4.

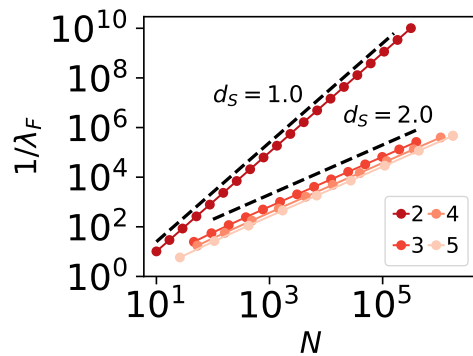


FIG. 4. **Fiedler scaling.** Scaling of the inverse of the Fiedler eigenvalue versus system size for different Bethe lattices and different values of  $z$  (see legend). Black dashed lines correspond to  $1/\lambda_F \sim N^{2/d_S}$ . Bethe lattices with  $z \geq 3$  present generic scaling with associated spectral dimension  $d_S = 2$ .

We now rigorously demonstrate that all Bethe lattices exhibit an identical spectral dimension  $d_S = 2$ . For convenience, let us consider a regular Cayley tree where all nodes present a branching ratio  $b$  and  $r$  iterations. The total number of nodes is

$$N_r = \frac{b^r - 1}{b - 1} \Rightarrow r = \frac{\log(Nb - N + 1)}{\log b}$$

Following the results of Erzan and Tuncer [4], we know that,

$$\lambda_F \sim (b - 1) b^{-r} = \frac{b - 1}{b^{\frac{\log(Nb - N + 1)}{\log b}}}$$

and thus,

$$\frac{1}{\lambda_F} \sim \frac{b^{\frac{\log(Nb - N + 1)}{\log b}}}{b - 1}$$

where the upper term simply involves the change of base formula  $\log_b a = \frac{\log_c a}{\log_c b}$ . Finally,

$$\frac{1}{\lambda_F} \sim N + \frac{1}{b - 1}$$

By comparison with the scaling form for  $1/\lambda_F$ ,  $d_S = 2$ , regardless of the value of  $b$ .

## 6. BARABÁSI-ALBERT NETWORKS

We have analyzed BA networks with subsequent values of  $m > 1$  for both cases  $\hat{L}$  and  $\hat{L}_{RW}$ . As shown in Figures 5 and 6, BA networks show no sign of scaling properties for  $m > 1$ , nor in the specific heat, where any plateau is present, nor in the analysis of the Fiedler eigenvalue, where only the network with  $m = 1$  presents a bona-fide scaling with  $d_S = 2$ .

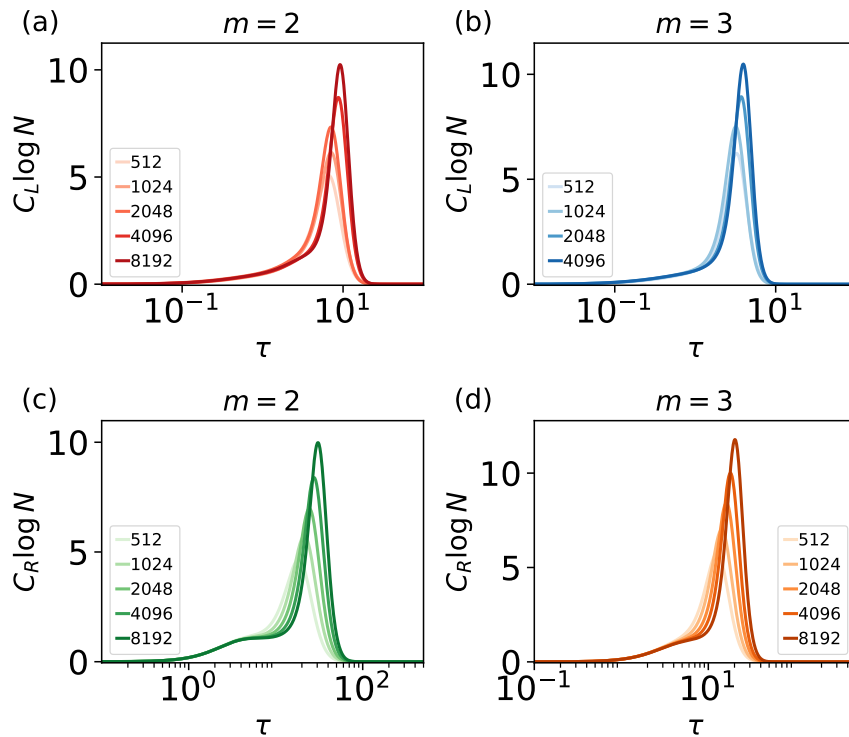


FIG. 5. **Barabási-Albert**. Specific heat versus system size for BA networks of different  $m$  for: (a)  $\hat{L}$ ,  $m = 2$ , (b)  $\hat{L}$ ,  $m = 3$ , (c)  $\hat{L}_{RW}$ ,  $m = 2$ , and (d)  $\hat{L}_{RW}$ ,  $m = 3$ . All cases show no plateau, evidencing the absence of scale-invariant properties of the networks.

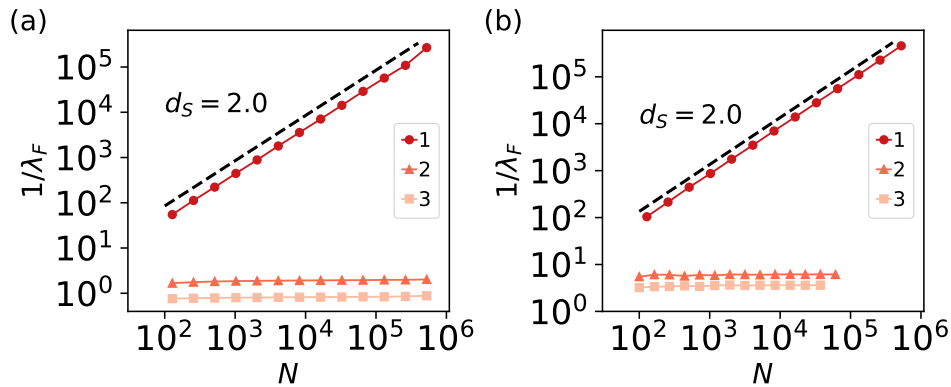


FIG. 6. **Spectral dimension.** Scaling of the inverse of the Fiedler eigenvalue versus system size for different Barabási-Albert networks and different values of  $m$  (see legend) by using (a) the Laplacian  $\hat{L}$  and (b) the normalized Laplacian  $L_{RW}$ . In both cases, only the case with  $m = 1$  is truly scale-invariant with spectral dimension  $d_s = 2$ .

### 7. $(u, v)$ -FLOWERS

The  $(u, v)$ -flowers are deterministic and recursive graphs [5]. Let us briefly describe how such networks are built: At step  $t = 0$ , the graph  $G(0)$  corresponds to a dimer, that is, two nodes connected by a link. The structure of successive  $G(t > 0)$  is driven by both the parameters  $u$  and  $v$ , together with  $1 \leq u \leq v$ .  $G(t)$  is built by replacing each link of  $G(t - 1)$  with two parallel links of, respectively, length  $u$  and  $v$ , as shown in Fig. 7.

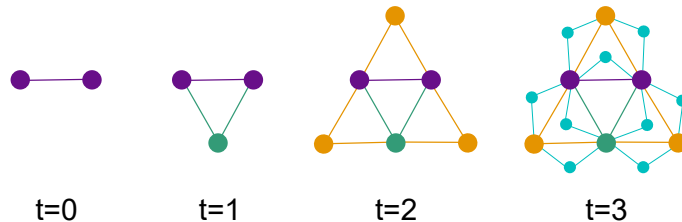


FIG. 7. Construction of the  $(1, 2)$ -flowers at steps  $t = 0, 1, 2, 3$ .

Such a procedure generates different types of graphs. Hence,  $(> 1, v)$ -flowers are known to exhibit finite Hausdorff dimension,  $d_H$ , while  $(1, v)$ -flowers have been called transfinite fractals (transfractals) and hold strong small-world properties with infinite Hausdorff dimension. In particular, all the derivations of  $d_H$  are based on rescaling analyses of the diameter of the graph  $L$  (e.g.,  $N(L + \ell) = e^{\ell \bar{d}_f} N(L)$ ,  $N$  number of nodes) instead of a multiplicative one (e.g.,  $N(bL) = b e^{d_f} N(L)$ ). However, we note that the general spectral dimension of both types of networks is  $d_s = \log(u + v) / \log(uv)$ , corresponding to the analysis of the Fiedler eigenvalue in Figure 9. Note also that, as expected for usual deterministic and recursively growing fractals [6], periodic oscillations are observed and detected by the specific heat as exemplified in Fig. 8.

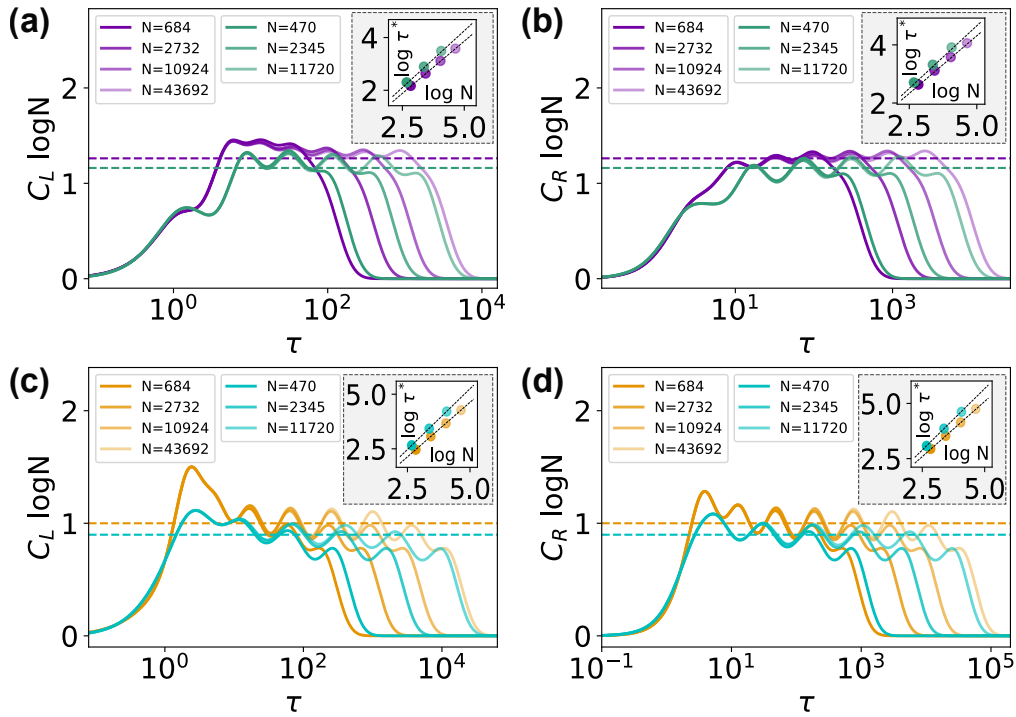


FIG. 8. **(u,v)-flowers.** Specific heat versus diffusion time  $\tau$  for different system sizes (see legend) for (1,3)-flowers (purple solid line) and (1,4)-flowers (green solid line) by using (a)  $\hat{L}$ , and (b)  $\hat{L}_{RW}$ , and (2,2)-flowers (orange solid line) and (2,3)-flowers (cyan solid line) by using (c)  $\hat{L}$  and (d)  $\hat{L}_{RW}$ . The colored horizontal dashed lines display the theoretical value of  $d_S/2$ , and the black dashed lines in the sub-panels show the theoretical scaling of  $C_F$  as suggested in the main text.

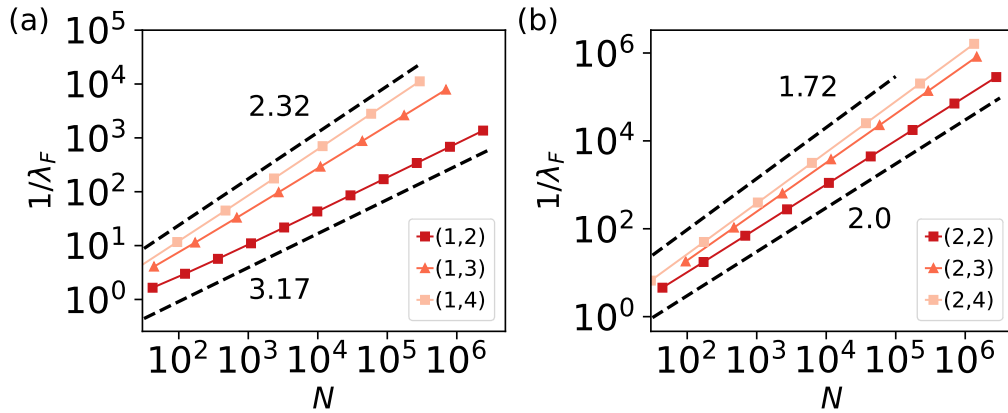


FIG. 9. **Spectral dimension for (u,v) networks.** Scaling of the inverse of the Fiedler eigenvalue versus system size for different  $(u, v)$  networks and different values of  $v$  (see legend) by using the Laplacian  $\hat{L}$  for (a)  $u = 1$ , (b)  $u = 2$ . In all cases, these networks are scale-invariant with variable spectral dimensions.

## 8. KIM AND HOLME NETWORKS

The analysis of standard BA networks with an extended mechanism to include a ‘triad formation step’ is particularly interesting to explore possible mechanisms to generate self-similar networks with  $d_S > 2$  [7]. Therefore, the generation mechanism proposed by Kim and Holme (KH) works by adding a new step to the preferential attachment rule as follows:

- (i) A vertex,  $v$ , with  $m$  edges is added at each time step. The growth time  $t$  is identified as the number of time steps.
- (ii) Preferential attachment rule (PA): Each edge of  $v$  is then linked to an already existing vertex with probability proportional to its degree, namely,  $P_i = \frac{\kappa_i}{\sum_j \kappa_j}$ .
- (iii) Triad formation (TF): After each PA step in which a new vertex  $v$  is added and some edge  $(u, v)$  is added, a triangle is closed with probability  $p$  by choosing a neighbor of  $u$ ,  $u_2$  and adding the edge  $(v, u_2)$ .

Here, we investigate whether KH networks show any power-law scaling of the Fiedler eigenvalue for different values of  $m$  and  $p$ . Let us highlight that the case with  $m = 1$  is rather trivial because it is impossible to close any triangle. Consequently, this latter mechanism will produce results identical to those of a simple BA network with  $m = 1$ . The results of the different types of KH networks (that is, the values of  $m$ ) for different TF probabilities are reported in Figure 10, making it evident that only KH networks with  $p = 1$  generate scale-invariant structures, as shown in the main text. In particular, the spectral dimension of the generated networks ranges from  $d_S = 2.57(1)$  and  $d_S = 3.65(1)$  for large values of  $m$ , as shown in Figure 11(b). Figure 11(a) and Figure 11(c) shows a specific example of these networks with  $m = 2$  and  $m = 3$ .

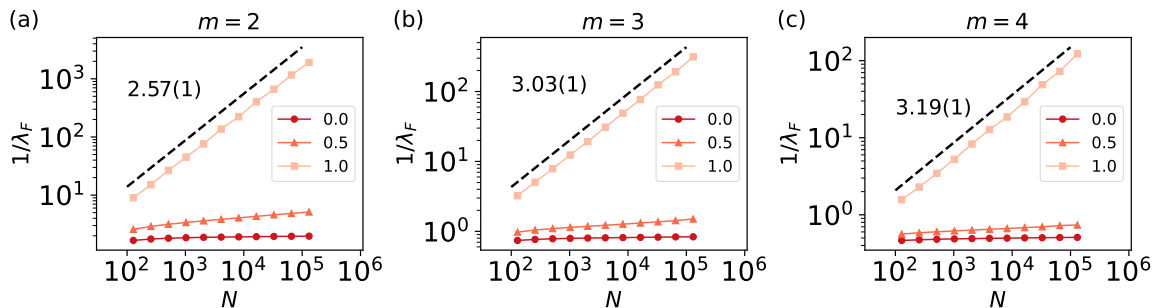


FIG. 10. **KH scale-invariant networks.** Scaling of the inverse of the Fiedler eigenvalue versus system size for different KH networks and different values of  $p$  (see legend) by using the Laplacian  $\hat{L}$  for (a)  $m = 2$ , (b)  $m = 3$ , and (c)  $m = 4$ . In all cases, only the case with  $p = 1$  is truly scale-invariant with variable spectral dimension.

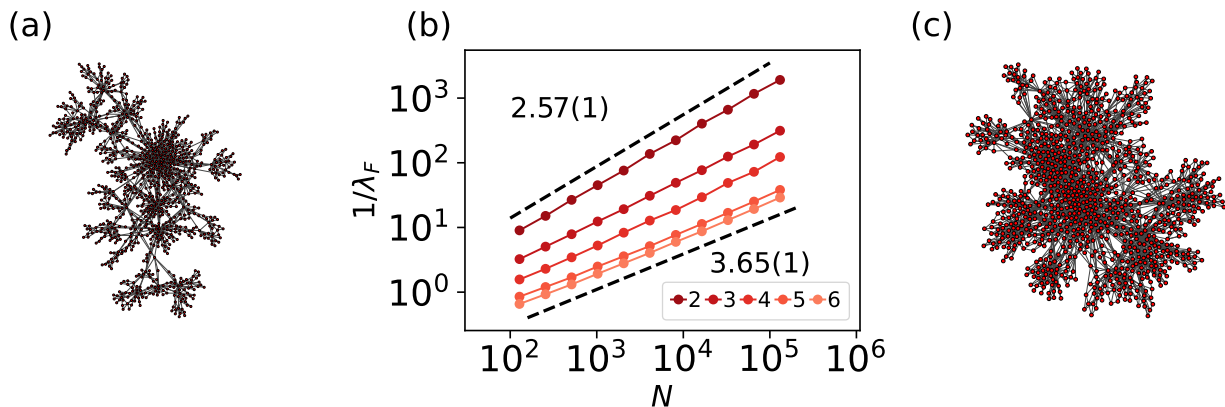


FIG. 11. **KH networks.** (a) KH network with  $m = 2$ ,  $p = 1$  and  $N = 1000$ . (b) Scaling of the inverse of the Fiedler eigenvalue versus system size for different KH networks with  $p = 1$  and varying  $m$  (see legend). The spectral dimension of the networks range from  $d_S = 2.57(1)$  to  $d_S = 3.65(1)$  for large values of  $m$ . (c) KH network with  $m = 3$ ,  $p = 1$  and  $N = 1000$ .

## 9. DYSON NETWORK

The Dyson graph is a weighted, fully connected, and deterministic graph. It was originally introduced by Dyson [8] to determine the occurrence of a phase transition in a one-dimensional chain with long-range interactions.

In the initial step, the network consists of a dimer with a weight link  $J(d = 1, t = 1, \sigma) = 4^{-\sigma}$ . Here,  $t$  is the iteration step, which is an integer  $\geq 1$ , such that the initial configuration of the dimer is called  $G(1)$ .  $d$  is the distance between two nodes and corresponds to the iteration step where they have been connected. In the next step, the graph is duplicated and all missing links are filled with a weight connection  $J(d = 2, t = 2, \sigma) = 4^{-2\sigma}$ . The same quantity is added to the weight of the old links, which now reads as  $J(d = 1, t = 2, \sigma) = J(d = 1, t = 1, \sigma) + 4^{-2\sigma}$ . Generalizing we get  $J(d, t - 1, \sigma) \rightarrow J(d, t, \sigma) = J(d, t - 1, \sigma) + J(t, t, \sigma)$ . Then it follows that each node will hold a unique degree  $w \equiv w_i = \sum_{i \neq j} J_{ij} = \sum_{d=1}^T 2^{d-1} J(d, T, \sigma)$ , where  $J(d, T, \sigma) = \sum_{l=d}^T J(l, t, \sigma)$ . Thus, the parameter  $\sigma$  can be adjusted to modulate the decay of the interaction strength. In particular, its value affects the resulting spectral dimension that can be written as  $d_S = 2/(2\sigma - 1)$ . Finally, we have to add that  $\sigma$  is bounded as follows:  $1/2 < \sigma \leq 1$ . The lower bound ensures the finite value of  $w$ . The upper bound does not let the inverse of the spectral gap grow faster than the system size.

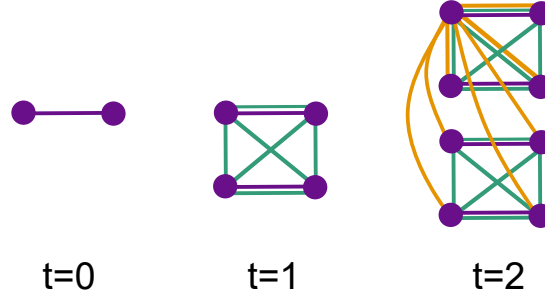


FIG. 12. Construction of Dyson graph at steps  $t = 0, 1, 2$ . For the sake of clarity, at step  $t = 2$ , only the new links involving the first node have been reported. The rest of the nodes will follow the same building rule.

Figure 13 shows the constant specific heat for different Dyson graphs with  $\sigma = 0.85$  and  $\sigma = 0.95$  and different system sizes. Note that these graphs can generate networks of arbitrary spectral dimension.

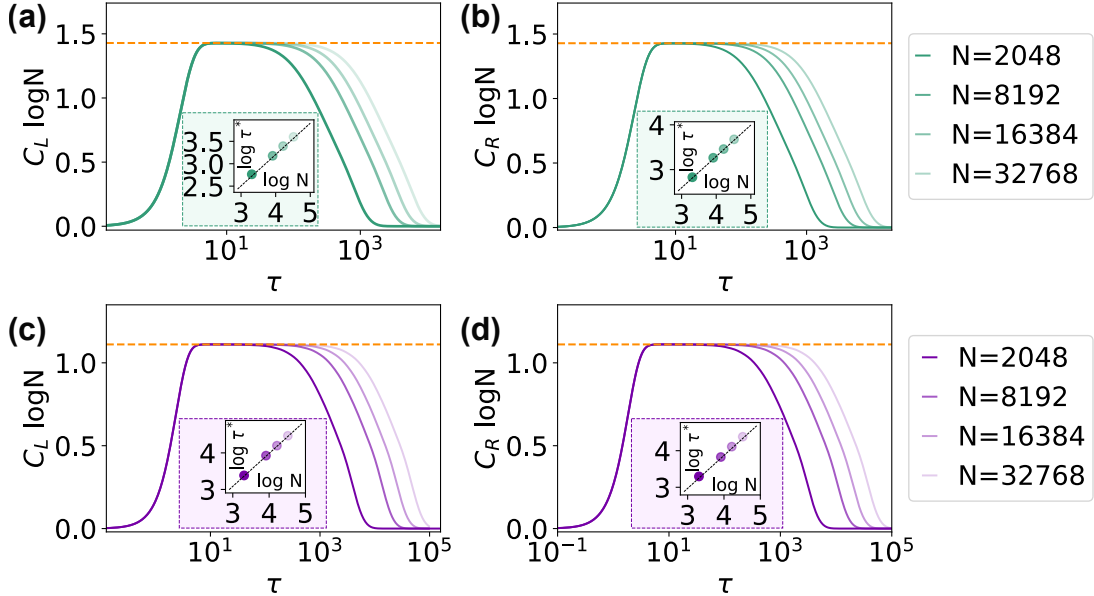


FIG. 13. **Dyson graphs.** Specific heat versus diffusion time  $\tau$  for different system sizes (see legend) for  $\sigma = 0.85$  using (a)  $\hat{L}$  and (b)  $\hat{L}_{RW}$ , and  $\sigma = 0.95$  using (c)  $\hat{L}$  and (d)  $\hat{L}_{RW}$ . The colored horizontal dashed lines display the theoretical value of  $d_S/2$ , and the black dashed lines in the sub-panels show the theoretical scaling of  $C_F$  as suggested in the main text.

## 10. HMN NETWORKS

We have also analyzed the synthetic hierarchical networks originally developed in [9]. These networks, called Hierarchic Modular Networks (HMNs), have been specifically generated to closely resemble the structure of real brain networks. In particular, HMN consists of  $N$  nodes or neurons and  $L$  links or synapses, organized into hierarchical levels for easy analysis. The HMN model that we exemplify here uses a bottom-to-top approach. First, we construct local fully connected modules and group them recursively by establishing new inter-modular links in a deterministic manner with a level-dependent number of connections (HMN).

Hence, the growing algorithm works as follows, as detailed in [9]:

- (i) At each hierarchical level  $l = 1, 2, \dots, s$ , different pairs of blocks are selected, each with size  $2^{l-1}M_0$ . All possible undirected  $4^{l-1}M_0^2$  connections between the two blocks are evaluated and established to avoid repetitions.
- (ii) The number of connections between blocks at each level is set a priori at a constant value  $\alpha$ .
- (iii) This method is stochastic in assigning connections, although the number of them (as well as the degree of the network) is fixed deterministically, being,

$$\langle \kappa \rangle = M_0 - 1 + \frac{2\alpha}{M_0}(1 - 2^{-s}).$$

Figure 14 shows the eigenvalue probability distribution for HMNs with  $M_0 = 2$  and different values of  $\alpha$ . Note the power-law scaling for small values of  $\lambda$ , where the number of oscillations increases with the number of hierarchical levels,  $s$ . Figure 15 shows the inverse of the Fiedler eigenvalue for different classes of HMN networks using fully connected cliques of size  $M_0 = 2$ ,  $M_0 = 3$ , and  $M_0 = 4$  as basal blocks. In particular, we observe that the spectral dimension of these specific networks continuously varies over the interval  $d_S \in (1.25, 2)$ .

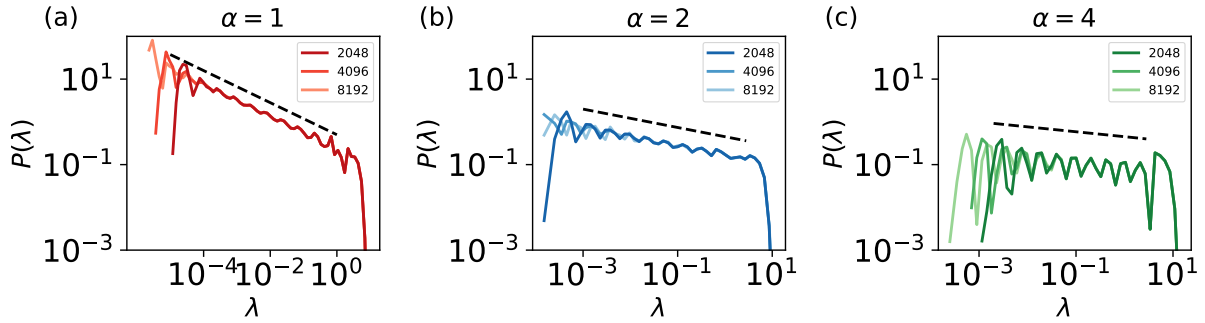


FIG. 14. **HMN eigenvalues.** Eigenvalue probability distribution for HMN networks with  $M_0 = 2$  and different system sizes (see legend) by using the Laplacian  $\hat{L}$  for (a)  $\alpha = 1$ , (b)  $\alpha = 2$ , and (c)  $\alpha = 4$ . All curves have been averaged over  $10^3$  independent realizations. Dashed lines represent the scaling  $P(\lambda) \propto \lambda^{d_S/2-1}$ .

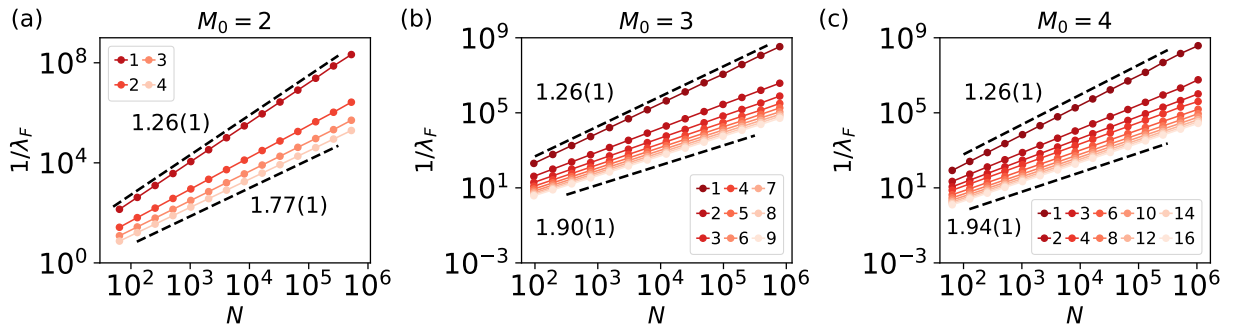


FIG. 15. **HMN spectral dimension.** Scaling of the inverse of the Fiedler eigenvalue versus system size for different HMN networks and different values of  $\alpha$  (see legend) by using the Laplacian  $\hat{L}$  for (a)  $M_0 = 2$ , (b)  $M_0 = 3$ , and (c)  $M_0 = 4$ . In all cases, HMN are scale-invariant networks with variable spectral dimensions.

Figure 16 shows the constant specific heat for different HMN networks for  $M_0 = 2$  and different values of  $\alpha$ . Note that all networks present a constant specific heat, either for  $C_L$  and  $C_R$  with the expected theoretical value of  $d_S$ .

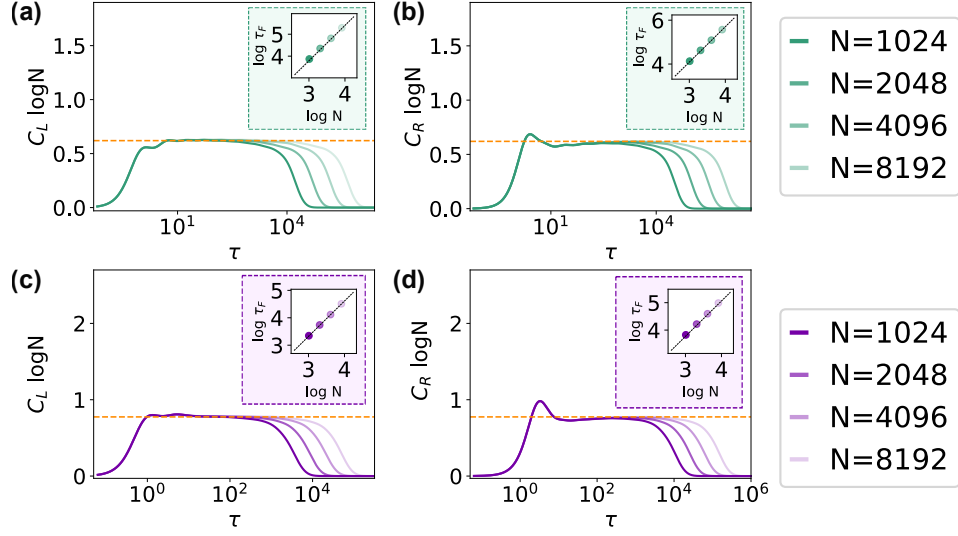


FIG. 16. **HMN graphs.** Specific heat versus diffusion time  $\tau$  for  $M_0 = 2$  and  $\alpha = 1$  using (a)  $\hat{L}$  and (b)  $\hat{L}_{RW}$ , and  $M_0 = 2$  and  $\alpha = 2$  using (c)  $\hat{L}$  and (d)  $\hat{L}_{RW}$ . The colored horizontal dashed lines display the plateau level, and the black dashed lines in the sub-panels show the theoretical scaling of  $C_F$ , as suggested in the main text. All curves have been averaged over  $10^3$  network realizations.

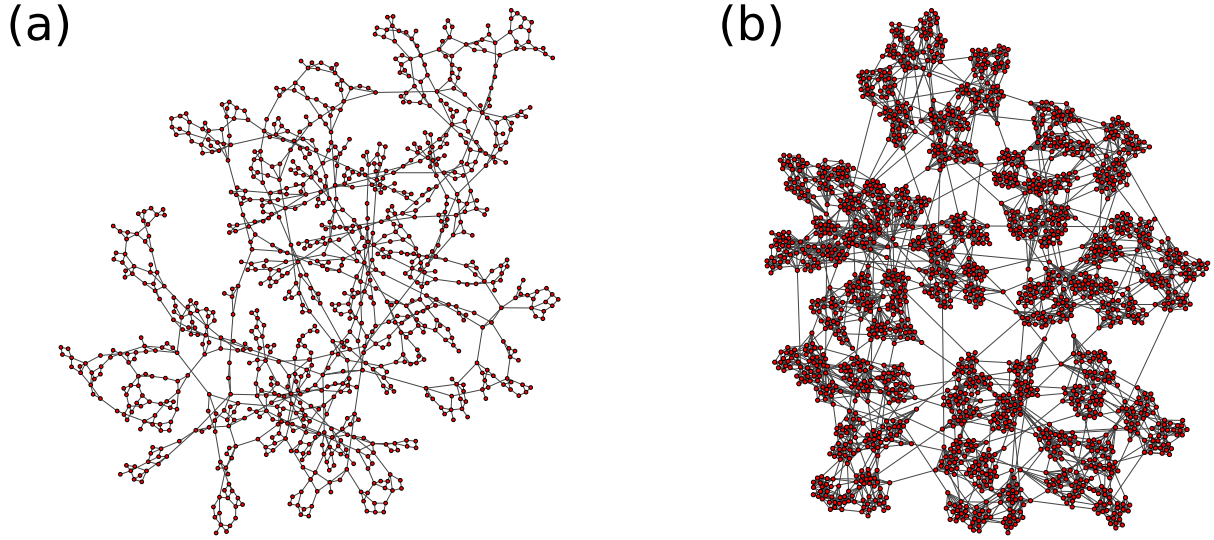


FIG. 17. **HMN networks.** (a) HMN network with  $M_0 = 2$ ,  $\alpha = 2$  and  $s = 9$  hierarchical levels. (b) HMN network with  $M_0 = 4$ ,  $\alpha = 10$  and  $s = 9$  hierarchical levels.

## 11. HUMAN CONNECTOME NETWORK

We have also analyzed the intrinsic structure of the Human Connectome Network (HC), a reconstruction of structural brain networks composed of hundreds of neural regions and thousands of white-matter fiber interconnections. This network consists of 998 nodes, each representing a mesoscopic population of neurons whose mutual connections are encoded by a symmetric weighted connectivity matrix. In particular, it is well-known that the HC is organized in modules and structured in a hierarchical fashion across many scales.

To uncover incipient scale-invariant features in HC, we have filtered the weighted HC matrix by imposing a threshold  $T$  below which the links are discarded (without performing any network binarization). We emphasize that, as a function of this threshold  $T$ , a random tree will always emerge, forming the backbone of the giant component of every network at the percolation threshold. However, here we observe that the network exhibits a kind of plateau near  $d_S \approx 2$  for  $T \in (2 \cdot 10^{-2}, 5 \cdot 10^{-2})$ , which is consistent with our previous results for HMN networks. Figure 18(a) shows the fraction of nodes belonging to the giant cluster ( $P_\infty$ ) and the remaining fraction of edges regarding their initial number ( $E_\infty$ ) when we sparsify the network. Note that at some specific value of  $T \approx 6 \cdot 10^{-2}$ , the resulting giant component corresponds to a random tree at the critical point of percolation. Instead, Figure 18(b) shows the resulting specific heat for the giant connected component of the sparsified network. Figure 19 shows the resulting networks for the different values of  $T$  analyzed in Figure 18(b).

Finally, to check whether the HC network actually exhibits scale-invariant properties, we performed iterative coarse-graining of the network using the LRG [10] and monitored the scaling of the Fiedler vector for different system sizes. We used the density matrix  $\rho(\tau)$  to define a network dendrogram as explicitly described in [10, 11]. Hence, by applying Ward's method to analyze the HC network clusters, it is possible to cut the dendrogram at different heights to generate reduced networks of smaller sizes, as shown in the main text.

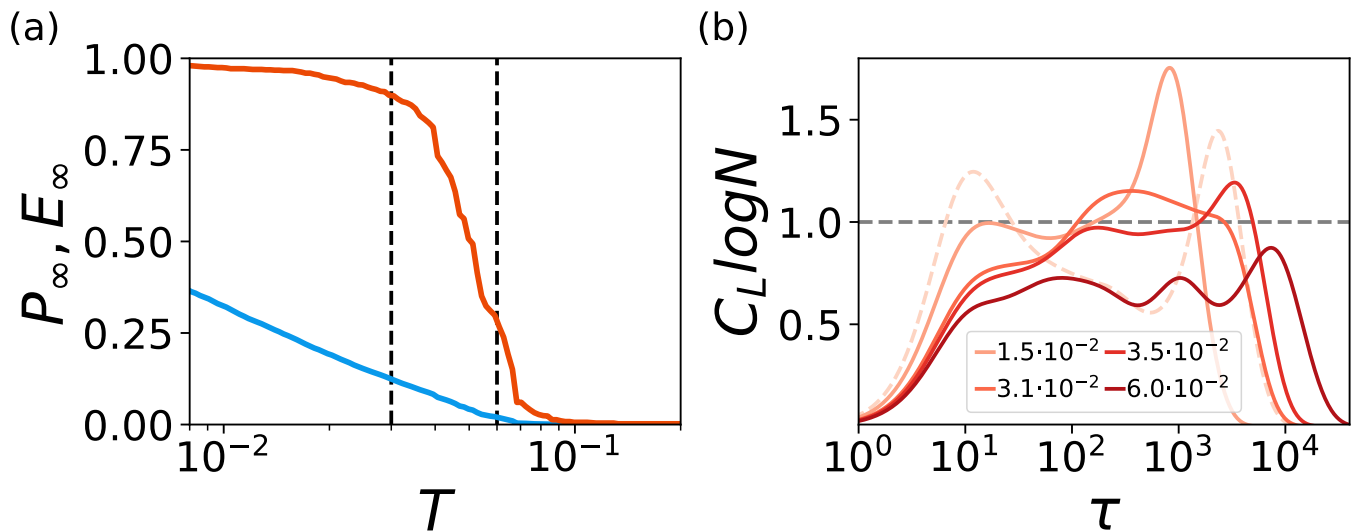


FIG. 18. (a) Giant cluster size ( $P_\infty$ ) and fraction of edges regarding the total original ones ( $E_\infty$ ) versus sparsification threshold  $T$ . The network shows a usual percolation phase transition for  $T \approx 0.6$ , while a non-trivial network structure still emerges with a non-vanishing giant component for threshold values  $T \in (2 \cdot 10^{-2}, 5 \cdot 10^{-2})$ . (b) Specific heat versus diffusion time for different values of  $T$  (see legend). Values of  $T$  within  $(2 \cdot 10^{-2}, 5 \cdot 10^{-2})$  are compatible with a spectral dimension  $d_S \approx 1.9(1)$ , while for  $T \approx 0.6$  a random tree with spectral dimension  $d_S = 4/3$  emerges, as expected for any percolation phase transition.

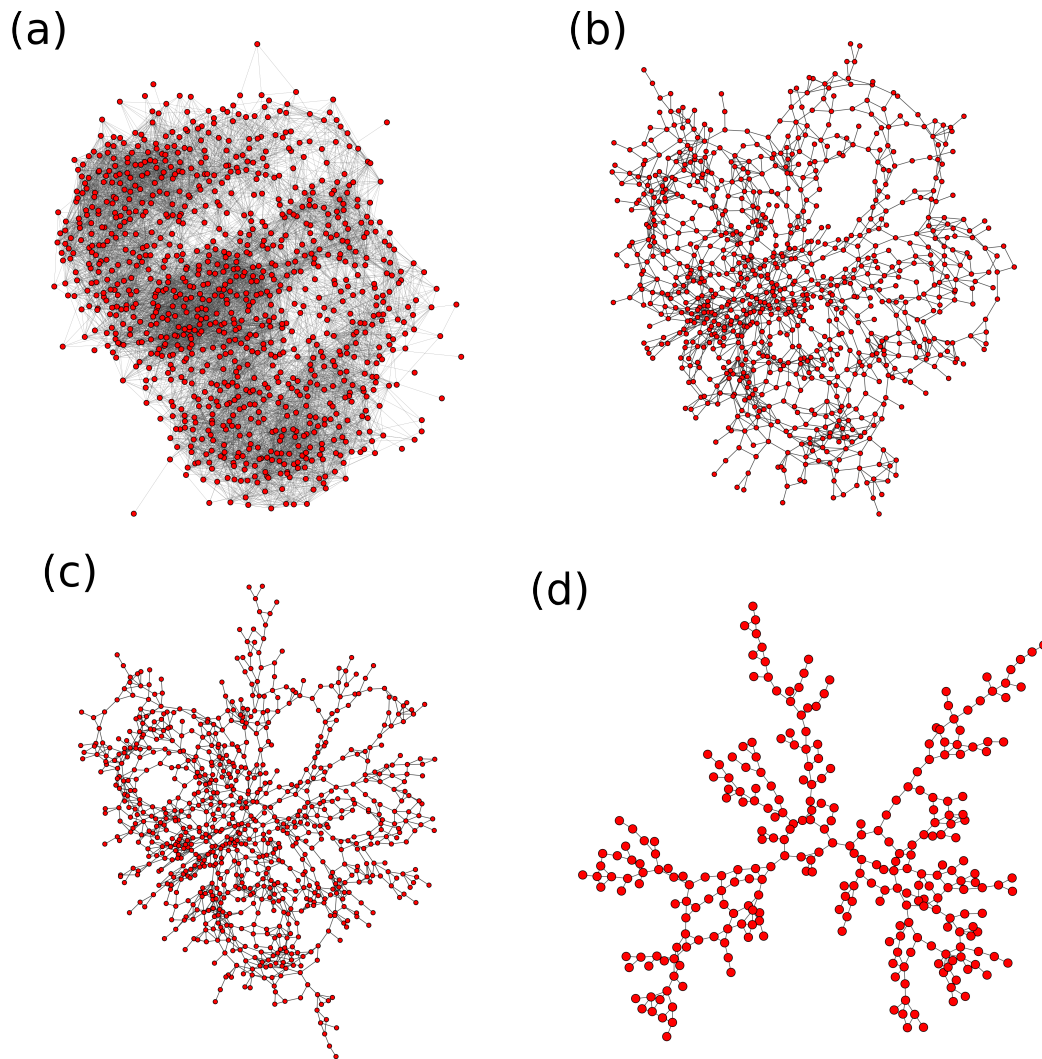


FIG. 19. Human Connectome network Giant cluster network for different threshold values. (a)  $T = 10^{-3}$ , (b)  $T = 3 \cdot 10^{-2}$ , (c)  $T = 3.5 \cdot 10^{-2}$ , and (d)  $T = 6 \cdot 10^{-2}$ . Note that, for the last case, the giant cluster of the network corresponds to a random tree as expected for a usual percolation phase transition.

## REFERENCES

- [1] K. C. Das, The laplacian spectrum, *Comput. Math. Appl.* **48**, 715 (2004).
- [2] S. N. Dorogovtsev and J. F. Mendes, *The nature of complex networks* (Oxford University Press, Oxford, 2022).
- [3] R. Burioni and D. Cassi, Random walks on graphs: ideas, techniques and results, *J. Phys. A* **38**, R45 (2005).
- [4] A. Erzan and A. Tuncer, Explicit construction of the eigenvectors and eigenvalues of the graph laplacian on the cayley tree, *Linear Algebra Its Appl.* **586**, 111–129 (2020).
- [5] H. D. Rozenfeld, S. Havlin, and D. Ben-Avraham, Fractal and transfractal recursive scale-free nets, *New J. Phys.* **9**, 175 (2007).
- [6] T. Vicsek, M. Shlesinger, and M. Matsushita, *Fractals in Natural Sciences* (World Scientific, Singapore, 1994).
- [7] P. Holme and B. J. Kim, Growing scale-free networks with tunable clustering, *Phys. Rev. E* **65**, 026107 (2002).
- [8] F. J. Dyson, Existence of a phase-transition in a one-dimensional ising ferromagnet, *Commun. Math. Phys.* **12**, 91 (1969).
- [9] P. Moretti and M. A. Muñoz, Griffiths phases and the stretching of criticality in brain networks, *Nat. Comm.* **4**, 2521 (2013).
- [10] P. Villegas, T. Gili, G. Caldarelli, and A. Gabrielli, Laplacian renormalization group for heterogeneous networks, *Nat. Phys.* **19**, 445–450 (2023).
- [11] P. Villegas, A. Gabrielli, A. Poggialini, and T. Gili, Multi-scale laplacian community detection in heterogeneous networks, arXiv (2023), 2301.04514.